

Comparing holographic principle inspired dark energy models

Vipin Chandra Dubey^{1*}, Umesh Kumar Sharma^{2†}

^{1,2} *Department of Mathematics,
Institute of Applied Sciences and Humanities,
GLA University, Mathura, U. P., 281406, India*

In this article, we have analysed holographic principle inspired dark energy models, namely Holographic dark energy (HDE) model, Tsallis Holographic dark energy (THDE) model and the Rényi holographic dark energy (RHDE) model by using the statefinder parameter diagnostic. We have compared these dark energy models by plotting the evolutionary trajectories of the first statefinder $r(z)$, second statefinder parameter $s(z)$, the statefinder parameter pairs (r, s) and (r, q) as well as the deceleration parameter $q(z)$ for the various parameter values of the respective dark energy models. It is observed from $q(z)$, $r(z)$ and $s(z)$ plots that the THDE model and RHDE model are not discriminated from Λ CDM model at the low redshift region, while the HDE model is well-differentiated from Λ CDM model at the low redshift region. Clear discrimination among these three dark energy models as well as from the Λ CDM model can be seen in the (r, s) and (r, q) planes.

I. INTRODUCTION

Presently, the expansion of our universe is accelerating, which is verified by various cosmological observations [1–6]. The dark energy (DE) is introduced for explaining this accelerated expansion in the framework of the standard cosmology, which is an obscure component with negative pressure [7–11]. Among various kinds of DE models, the cosmological constant model i.e. Λ CDM model is the simplest one [12–16]. For Λ CDM model, time-independent equation of state (EoS) $\omega_\Lambda = -1$, but it faces theoretical problems, specifically the fine tuning problem as well as the coincidence problem [13, 17, 18]. To get alleviation from such issues, numerous dynamical DE models are given as a choice such as tachyon [19], quintessence [20, 21], k -essence [22, 23], phantom [24] and Chaplygin gas [25].

Inspired by the holographic principle (HP) [26–29], the holographic dark energy (HDE) model was proposed by Li [30] in 2004. According to HP, the number of degrees of freedom for a system does not depend on the volume but its bounding area. The accelerated expansion phase of the Universe can be explained by the HDE [31, 32]. In anticipation of quantum modification for HDE, Tsallis and Cirto produce Tsallis entropy, which is a generalization of the Boltzmann-Gibbs (BG) entropy to non-extensive systems [33–35]. Being peculiar behaviour of the Universe and long-range aspects of gravity. A generalized entropy formalism has been considered for investigating the peculiar behaviour of the Universe and long-range aspects of gravity, which inspires us to a decent consent with gravity and its associated problems [36, 37].

Different entropies are also used for the investigation of the gravitational and cosmological scenario. Recently, two new forms of DE models based on HP, Tsallis and Rényi [38, 39] entropy are proposed by Tavayef et. al [40] and by Moradpour et. al [41], known as Tsallis holographic dark energy (THDE) and Rényi holographic dark energy (RHDE), respectively. Both the THDE and RHDE might be consistently called HP inspired dark models for simplicity. These models of HDE can be used to clarify or explain the cosmic acceleration of the universe [44–61].

The DE phenomenon can be explained by many DE models. Hence it becomes very important to distinguish among various vying DE models. In this way, Sahni et al. [62] and Alam et al. [63] introduced a significant geometrical indicative, namely statefinder pair (r, s) for removing the degeneracy in present values of q and H for different DE models. It is also used widely to recognise different models of modified theories of gravity. Since we get distinct evolutionary trajectories in (s, r) plane for different DE models. The statefinder parameters are analysed in [64–71]. The statefinder parameter diagnostic is also used to discriminate various DE models such as the Ricci dark energy (RDE), the new HDE, the new ADE and the original HDE model [72].

Motivated by the work of ref. [72], in this paper, we compare the original HDE model with some newly proposed DE models such as the Tsallis holographic dark energy (THDE) model and Rényi holographic dark energy (RHDE) model through the statefinder parameters $(r - s)$ diagnostic. In Sect. 2, we reviewed briefly the HP inspired DE models. In Sect. 3 we diagnosed these HDE models with the deceleration parameter q , and the statefinder. The conclusion is given in Sect. 4.

*vipin.dubey@gla.ac.in

†sharma.umesh@gla.ac.in

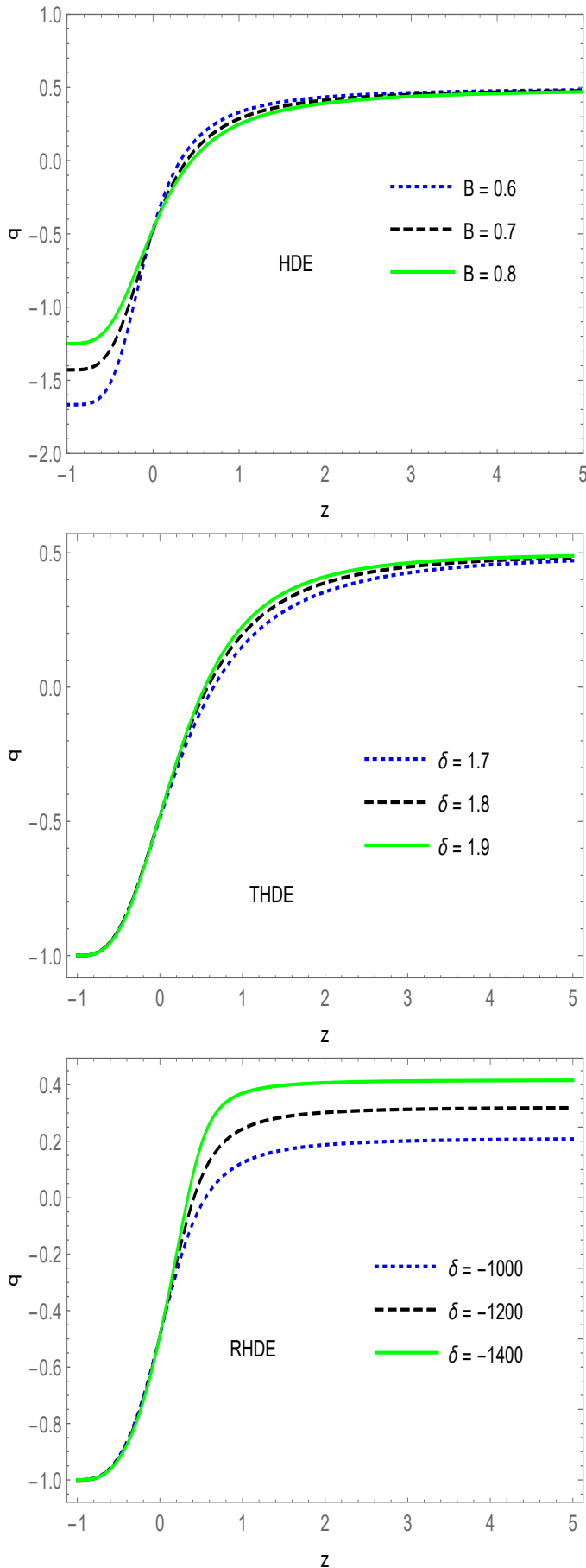


FIG. 1: The evolutionary behaviours of the q (deceleration parameter) versus z (redshift) for HDE, THDE and RHDE Models. Here, $\Omega_D(z=0) = 0.73$, $H(z=0) = 70$, $\omega_D(z=0) = -0.90$

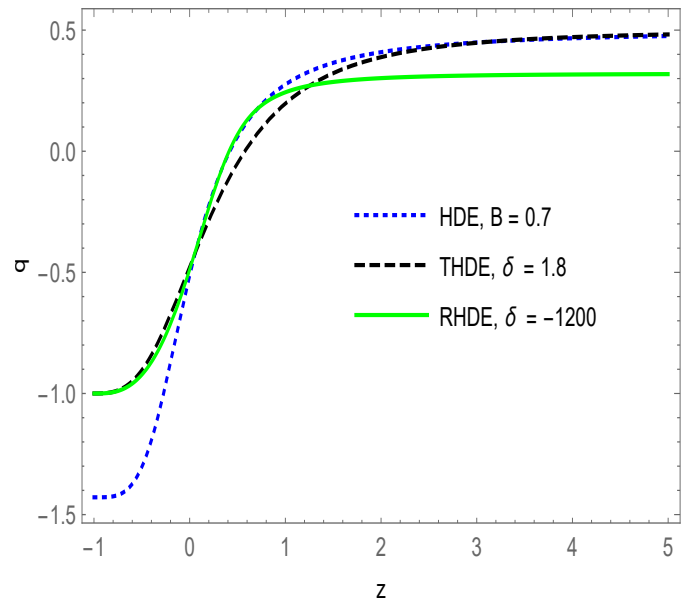


FIG. 2: Comparison of evolutionary behaviour of q for the HP inspired DE models. Here, $\Omega_D(z=0) = 0.73$, $H(z=0) = 70$, $\omega_D(z=0) = -0.90$

II. HOLOGRAPHIC PRINCIPLE INSPIRED DE MODELS

A. The HDE model

Considering a spatially flat Friedmann Robertson Walker Universe accommodating matter and dark energy (assuming a flat Universe in the complete manuscript), the Friedmann equation is given as

$$H^2 = \frac{1}{3M_p^2} (\rho_m + \rho_D), \quad (1)$$

where ρ_m , ρ_D represent the energy densities for matter and DE, respectively, and $M_p = \frac{1}{\sqrt{8\pi G}}$ is the reduced Planck mass. H is the Hubble parameter. For the HDE model [26, 73], $\rho_D = 3B^2 M_p^2 L^{-2}$, where L is the largest IR cut-off and B is a dimensionless constant. Now,

by taking the future event horizon as IR cut-off L , we have:

$$R_h = a \int_a^\infty \frac{da'}{H(a')a'^2}, \quad (2)$$

Eq. (1) can be written as:

$$1 = \Omega_D + \Omega_m, \quad (3)$$

Where $\Omega_m = \Omega_m^0 H_0^2 H^{-2} a^{-3}$ and $\Omega_D = B^2 H^{-2} R_h^{-2}$ be the relative energy densities of matter and DE, respectively, which are expressed as fractions of the

critical density $\rho_c = 3M_p^2 H^2$. Here, H_0 and Ω_{m0} are the present values of the Hubble parameter H and the matter density parameter Ω_m . Now, by using $R_h = B/H\sqrt{\Omega_D}$ and Eq. (2), we have:

$$\int_x^\infty \frac{da'}{H(a')a'} = \frac{B}{H(a)a\sqrt{\Omega_D}}, \quad (4)$$

where $x = \log a$. Now from the Friedmann equation, we have [66] :

$$\frac{1}{H(a)a} = \sqrt{a(1 - \Omega_D)} \frac{1}{H_0 \sqrt{\Omega_m^0}}, \quad (5)$$

From Eq. (4) and Eq. (5), we get the relation

$$\int_x^\infty e^{x'/2} \sqrt{1 - \Omega_D} dx' = B e^{x/2} \sqrt{\frac{1}{\Omega_D}} - 1. \quad (6)$$

Now, differentiating Eq. (6) with respect to $x = \log a$, we have

$$\Omega'_D = \Omega_D (1 - \Omega_D) \left(\frac{2\sqrt{\Omega_D}}{B} + 1 \right). \quad (7)$$

Where the prime represents the differential coefficient with $x = \log a$. Also, the energy conservation law, $\dot{\rho}_D + 3H(\omega_D + 1)\rho_D = 0$, the equation of state (EOS) parameter of the HDE, $\omega_D \equiv p_D/\rho_D$, can be given by [66]:

$$\omega_D = -\frac{1}{3} - \frac{2\sqrt{\Omega_D}}{3B}, \quad (8)$$

B. The THDE model

Newly, another form of non-extensive and HP inspired dark model has been proposed in [40], and the energy density for the THDE is defined as

$$\rho_D = BH^{4-2\delta}, \quad (9)$$

where the parameter B is unknown and δ is the non-extensive real parameter, which quantifies the degree of non-extensive [33, 34, 36, 42]. Taking the time derivative of $\Omega_D \equiv \frac{\rho_D}{3M_p^2 H^2}$ on both sides with respect to $x = \log a$, we get

$$\Omega'_D = \frac{3(\delta - 1)\Omega_D(1 - \Omega_D)}{1 - (2 - \delta)\Omega_D}, \quad (10)$$

So, the THDE equation of state (EoS) parameter is inferred as

$$\omega_D = \frac{\delta - 1}{(2 - \delta)\Omega_D - 1} \quad (11)$$

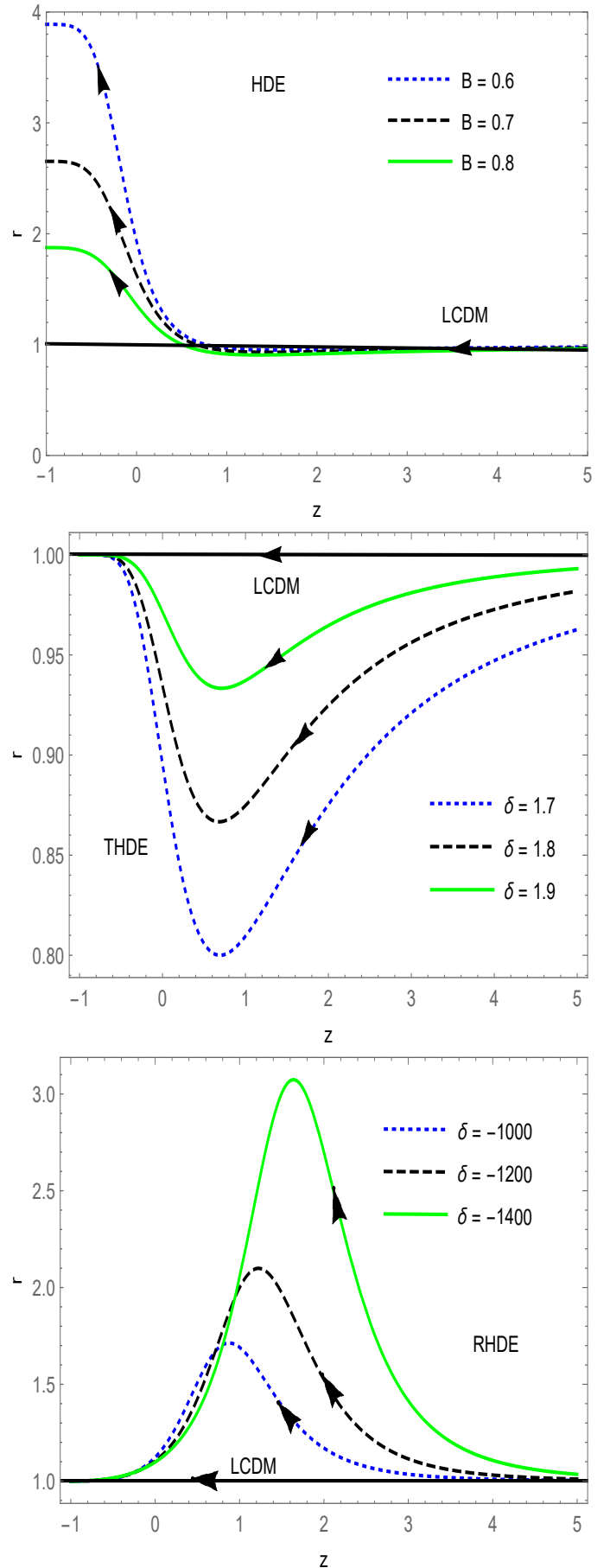


FIG. 3: The evaluation of the first statefinder parameter r versus redshift parameter z for HDE, THDE and RHDE Models. Here, $\Omega_D(z=0) = 0.73$, $H(z=0) = 70$, $\omega_D(z=0) = -0.90$.

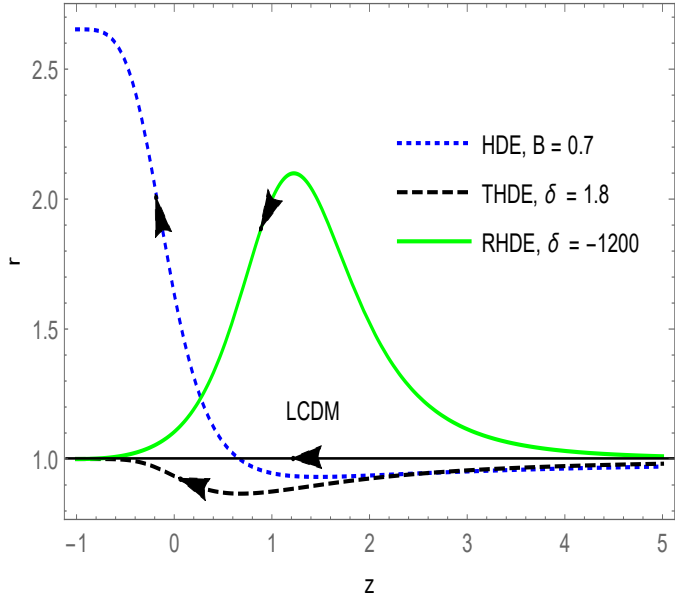


FIG. 4: Comparison of evolutionary trajectories of the first statefinder parameter r for the HP inspired DE models. Here, $\Omega_D(z=0) = 0.73$, $H(z=0) = 70$, $\omega_D(z=0) = -0.90$.

C. The RHDE model

Furthermore, one more form of DE based on Rényi entropy and HP inspired DE has been suggested in [41], and the energy density for the RHDE is given as

$$\rho_D = \frac{3B^2 H^2}{8\pi \left(\frac{\pi\delta}{H^2} + 1\right)}, \quad (12)$$

where the value of a numerical constant B^2 is taken as $B^2 = \left(\frac{\pi\delta}{H_0^2} + 1\right)(1 - \Omega_{m0})$ [36]. Taking the time derivative of $\Omega_D \equiv \frac{\rho_D}{3M_p^2 H^2}$ on both sides with respect to $x = \log a$, we get

$$\Omega'_D = -\frac{3\pi B^2 \delta H^2 (\Omega_D - 1)}{(\pi\delta + H^2)(\pi\delta(2\Omega_D - 1) + H^2(\Omega_D - 1))}, \quad (13)$$

So, for the RHDE, the EoS parameter is given as

$$\omega_D = -\frac{\pi\delta}{\pi\delta(2\Omega_D - 1) + H^2(\Omega_D - 1)}, \quad (14)$$

III. STATEFINDER DIAGNOSTIC

Before the presence of the statefinder parameters (r), (s) and the statefinder pair (s, r) and (q, r), one may differentiate various DE models with the help of the

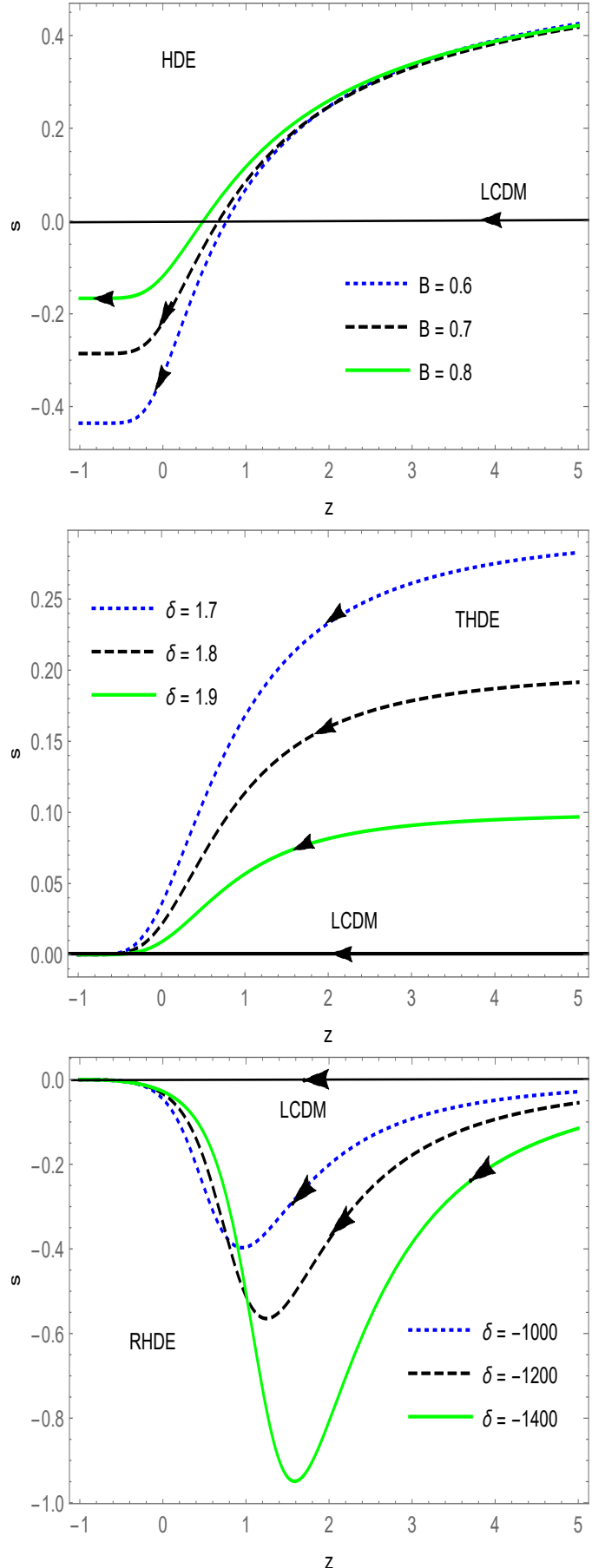


FIG. 5: The evolutionary trajectories of the second statefinder parameter s versus redshift parameter z for HDE, THDE and RHDE models. Here, $\Omega_D(z=0) = 0.73$, $H(z=0) = 70$, $\omega_D(z=0) = -0.90$.

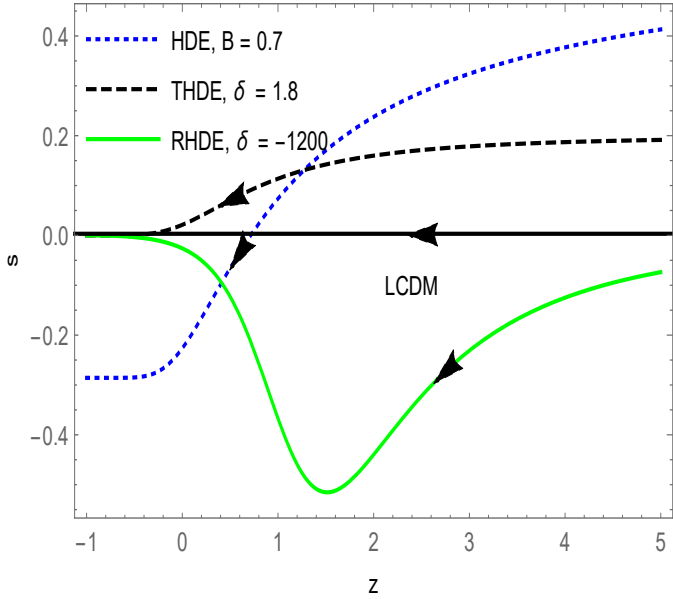


FIG. 6: Comparison of evolutionary trajectories of the second statefinder parameter s for the HP inspired DE models. Here, $\Omega_D(z=0) = 0.73$, $H(z=0) = 70$, $\omega_D(z=0) = -0.90$.

evolution of the deceleration parameter $q(z)$. Therefore, we take into consideration the evolution of q for the aforementioned 3 HP inspired DE models in this work.

The deceleration parameter q can be expressed in a spatially flat Universe in terms of Ω_D [66].

$$q = \frac{1}{2} + \frac{3\omega_D\Omega_D}{2} \quad (15)$$

It is important to mention here that for all three models i.e. HDE, THDE and RHDE, we fix $\Omega_D(z=0) = 0.73$, $H(z=0) = 70$, $\omega_D(z=0) = -0.90$. For the HDE model, parameter B is taken as (0.6, 0.7, 0.8) [72, 74]. For the THDE model, the model parameter δ is taken to be (1.7, 1.8, 1.9) [67, 69]. The parameter δ in the RHDE model is taken to be (-1000, -1200, -1400) [75].

The evolutionary behaviour of the deceleration parameter q is plotted in Fig. 1, for all three HP inspired DE i.e. the HDE, THDE and RHDE models. We observe from the figure that for the HDE model the evolutionary behaviour of q can be discriminated with each other for various values of the model parameter B in the low-redshift region while it can not be discriminated in high-redshift region. For the THDE model, it is clear from the figure that the evolutionary behaviour of q can not be discriminated with each other for different values of the model parameter δ in the low-redshift region as well as in high-redshift region. Also, for the RHDE model, it is clear from the figure that the evolutionary

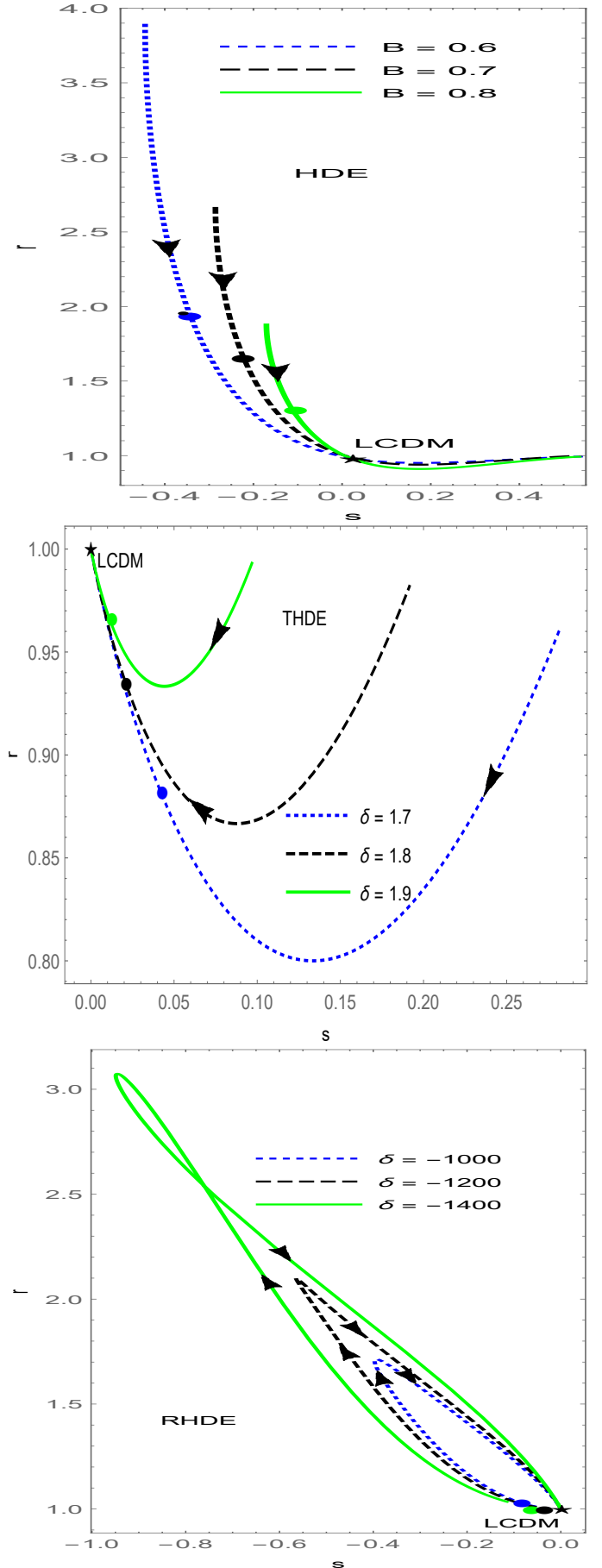


FIG. 7: The evolutionary trajectories of r versus s for HDE, THDE and RHDE models. Here, $\Omega_D(z=0) = 0.73$, $H(z=0) = 70$, $\omega_D(z=0) = -0.90$.

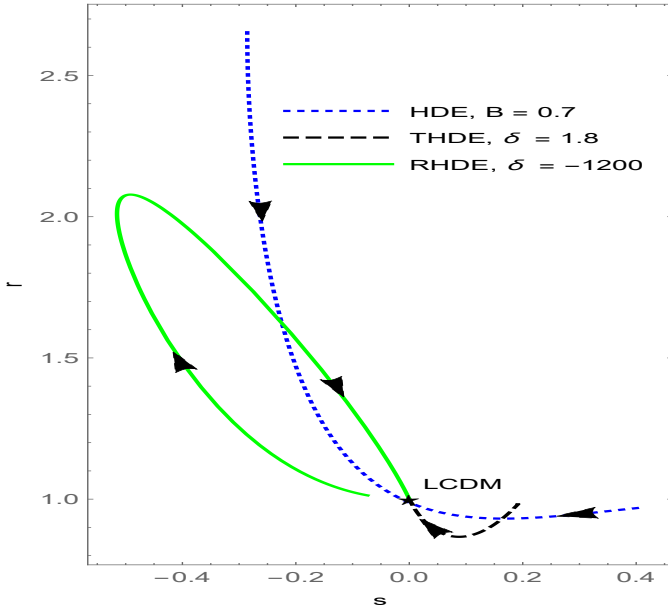


FIG. 8: Comparison of evolutionary trajectories of the (r, s) pair plane for the HP inspired DE models. Here, $\Omega_D(z=0) = 0.73$, $H(z=0) = 70$, $\omega_D(z=0) = -0.90$.

behaviour of q can not be discriminated with each other for different values of the model parameter δ in the low-redshift region but can be differentiated in high-redshift region. Although, the behaviour of deceleration parameter q for all three DE model is in toe with the observational results, which depicting the deceleration to acceleration phase of the universe. Similarly, we moreover graph the deceleration parameter q evolution of the three HP inspired DE models in Fig. 2. From $q(z)$ diagnostic, it is difficult to differentiate among these DE models.

For discriminating among different DE models, now we investigate the statefinder parameter, which is constructed from the scale factor by taking its derivatives up to the third order. The statefinder pair $\{r, s\}$ is constructed from the space-time metric directly and it gives a very comprehensive overview of the dynamics of the Universe and subsequently the nature of the DE. The statefinder parameters are given as: [62, 63]

$$r = \frac{\ddot{a}}{aH^3} \quad (16)$$

$$s = \frac{r-1}{3(q-\frac{1}{2})} \quad (17)$$

The statefinder parameters r and s can be expressed in terms of the EoS parameter and energy density as given below:

$$r = 1 + \frac{9}{2}\omega_D(1+\omega_D)\Omega_D - \frac{3}{2}\omega_D'\Omega_D \quad (18)$$

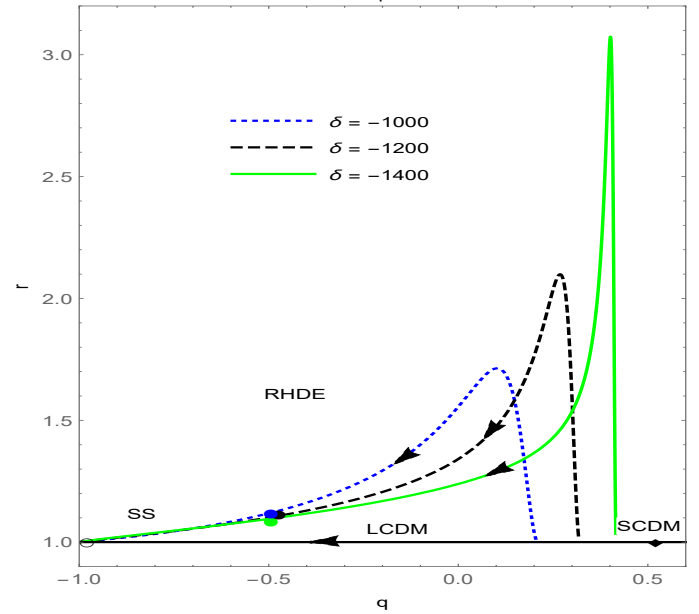
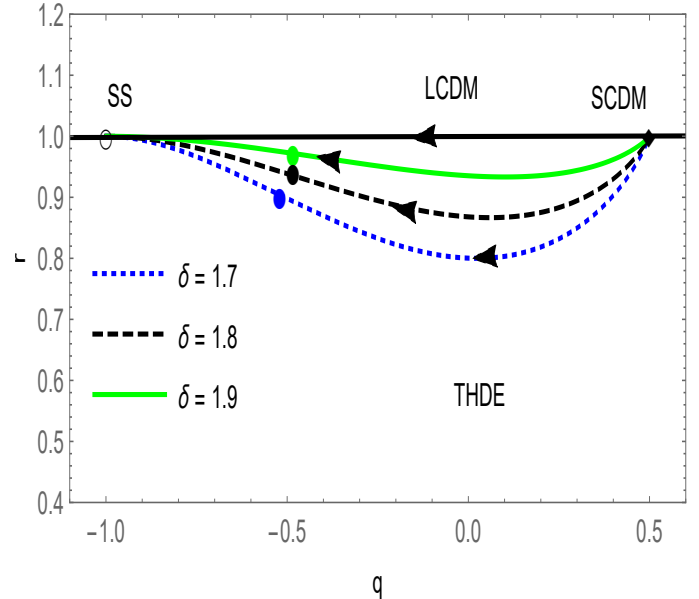
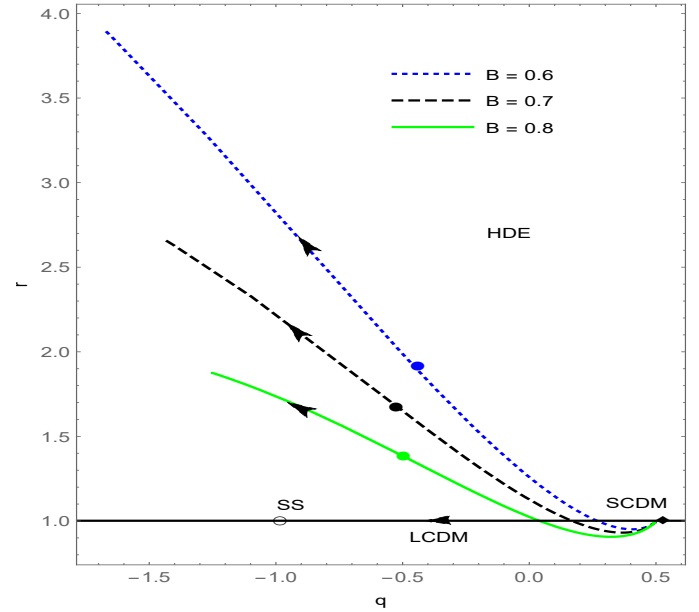


FIG. 9: The evolutionary behaviour of the (r, q) pair for HDE, THDE and RHDE Model. Here, $\Omega_D(z=0) = 0.73$, $H(z=0) = 70$, $\omega_D(z=0) = -0.90$.

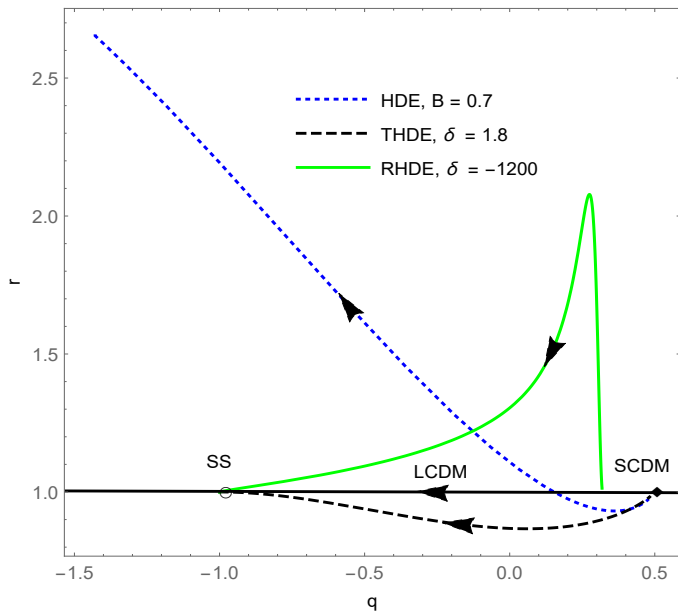


FIG. 10: Comparison of evolutionary trajectories of the (r, q) pair for the HP inspired DE models. Here, $\Omega_D(z=0) = 0.73$, $H(z=0) = 70$, $\omega_D(z=0) = -0.90$.

$$s = 1 + \omega_D - \frac{1}{3} \frac{\omega_D'}{\omega_D}, \quad (19)$$

Where the prime represents the differential coefficient with $x = \ln a$. The evolutionary behaviour of the first statefinder parameter r with z is shown in Fig. 3, for all three HP inspired DE models with different model parameter values compared with Λ CDM model. From Fig. 3 to Fig. 10, the arrows indicate the evolution directions.

We see from Fig. 3, that for HDE model the evolutionary behaviour of the first statefinder parameter r can be well discriminated from Λ CDM model (denoted by black solid line $r = 1$ in the figure) in the region $-1 \leq z \leq 1$ for different values of the model parameter c while it can not be distinguished from Λ CDM model in the region $1 \leq z \leq 5$. For the THDE and RHDE model, it is clear from the figure that the evolutionary behaviour of r for different values of the model parameter δ is distinct from Λ CDM model in the region $-0.5 \leq z \leq 5$ but can not be discriminated from Λ CDM model in the region $-1 \leq z \leq -0.5$. A straight comparison between the Λ CDM model and these three HP inspired DE models with the first statefinder parameter r can be seen in Fig. 4. The differentiation of these three DE models are clearly observed in the region $-0.5 \leq z \leq 5$. The difference between the HDE model and the Λ CDM model becomes clearer in the range $-1 \leq z \leq -0.5$, while THDE and RHDE models are not distinct from Λ CDM model in this range.

Fig. 5, shows the evolution of the second statefinder

parameter s versus z of the three HP inspired DE models for different values of model parameters, also compared with the Λ CDM model (denoted by black solid line $s = 0$ in the figure). For the HDE model, the evolutionary trajectories show legible separation from the Λ CDM model in the region $-1 \leq z \leq 5$. While, for the THDE and the RHDE models, the $s(z)$ curves are not distinct from Λ CDM model in the region $-1 \leq z \leq -0.5$, for different values of the model parameter δ . These DE models separate more distinctly for different values of model parameters in the region $-1 \leq z \leq -0.5$. Fig. 6, compares the HDE, THDE and the RHDE models with the second statefinder parameter $s(z)$ from the Λ CDM model. The clear differentiation of these DE models can be seen in the region $-0.5 \leq z \leq 5$. The evolutionary trajectories of both first and second statefinder parameters shows that these DE models are separate distinctively in the region $-0.5 \leq z \leq 5$, but THDE, RHDE models are not differentiated and approaches to Λ CDM model in the region $-1 \leq z \leq -0.5$.

To break this degeneracy, the evolutionary trajectories for the HDE, THDE and the RHDE models are plotted in Fig. 7 for different parameter values in (r, s) plane. The point (s_0, r_0) denotes the present value of the statefinder parameters, which are marked as the dotted circle in the figures. The fixed point $(0, 1)$ presented by the star in these figures represents the Λ CDM. We can discriminate DE models with the statefinder diagnostic (r_0, s_0) , if we have accurate information of (r_0, s_0) which can be retrieved from the future high precision observational data.

We have quintessence if the parameters $(r < 1, s > 0)$, while if $(r > 1, s < 0)$, we have Chaplygin gas model. From Fig. 7 & 8, we clearly observe that the trajectory of (r, s) plane of HDE model shows quintessence as well as Chaplygin gas behaviour at an early time for different values of model parameter c and finally reaches to Λ CDM in the far future. The evolution of the (r, s) plane for the THDE model shows that the curve lies in the quintessence region at early time and finally approaches to Λ CDM at late time. While the evolutionary trajectories of the statefinder pair (r, s) of the RHDE model show only the Chaplygin gas behaviour at an early time and forms swirl before reaching to Λ CDM in the remote future. Which is quite different from the other two DE models. Fig. 7, also depicts that the model parameters of these DE models not only discriminate the present values of $\{s, r\}$ but also differentiate the evolutionary trajectory in (r, s) plane.

As a complementarity for the diagnostic, we also plot the evolutionary trajectories of the statefinder pair $(q-r)$ in Fig. 9. The point $(0.5, 1)$ represents the SCDM, that is the matter-dominated Universe in this graph, and the fixed point $(-1, 1)$ represents SS- the de Sitter expansion i.e. the steady-state, which are marked by filled diamonds and the empty circle, respectively. Important

point to mention here that the black solid horizontal line starting from the fixed point of SCDM model and ending at the fixed point of SS model denotes evolution of the Λ CDM model, which divides the $q - r$ plane into 2 parts. The upper half is occupied by Chaplygin gas model and the lower half contain quintessence models. We also observe the signature flip in the value of q from +ve to -ve, which explains the recent phase transition successfully. For the HDE model, we can see that both the Λ CDM scenario and HDE model start evolving from the same point in the past ($r = 1, q = 0.5$) which corresponds to a matter-dominated SCDM Universe, and crosses the point ($q = -1, r = 1$) in the future, which corresponds to a steady-state cosmology (SS) the de Sitter expansion. For the THDE model evolutionary trajectories start evolving from SCDM i.e. matter-dominated Universe ($q = 0.5, r = 1$) in the past, and their evolution ends at the same point ($q = -1, r = 1$) in the future for different parameter values. For the RHDE model, evolutionary trajectories start evolving from different points in the past, and their evolution ends at the point ($q = -1, r = 1$) in the future for different parameter values. Thus, the ‘distance’ from this model to the de Sitter expansion (SS) can be easily identified in this diagram. A direct comparison of these DE models in the $(q - r)$ plane is shown in Fig. 10.

The evolution trajectories of the statefinder pair ($r - q$) of the HDE model show both quintessence and the Chaplygin gas behaviour. The THDE model always lies in the quintessence region. The evolutionary trajectory of the RHDE model corresponds to the Chaplygin gas model.

IV. CONCLUDING REMARKS

Many dynamical DE models have been proposed so far in the literature, inspired by the HP and various entropy formalisms. Hence, it is of great interest to differentiate these HP inspired DE models with the observational results. Although, especially, in the low-redshift region, these models are degenerate with each other to some extent. We compare three important HP inspired DE models, i.e., the THDE, HDE and RHDE and we use the statefinder parameter analysis to differentiate them in this work.

We observe from the $q(z)$ evolution that THDE and RHDE models can not be discriminated in the low-redshift region while HDE model can be discriminated in this region. Interestingly, all three DE models repre-

sent the decelerating to accelerating universe for different parameter values. Since most of the observational results are mainly within the low red-shift region (generally $z \leq 1$). For the more clear discrimination among these DE models in the low-redshift region, it is important to use some quantities with higher-order differential coefficients of the scale factor. We observe that the first and second statefinder parameters $r(z)$ and $s(z)$ are very helpful for this purpose.

We observe from the $r(z)$ and $s(z)$ analysis that THDE and RHDE models can not be differentiated in the low-redshift region from the Λ CDM model but can be discriminated in the range $-0.5 < z < 5$ from the Λ CDM model. It is clear that both the THDE and RHDE approach to the Λ CDM model in the low-redshift region. The RHDE and HDE models can not be discriminated in the high-redshift region from the Λ CDM model in $r(z)$ plane, while all the three DE models can be well discriminated from Λ CDM model in $s(z)$ plane for the various parameter values in the high red-shift region.

For all three HP inspired DE models i.e. THDE, HDE and RHDE a direct comparison in (r, s) and (r, q) plane has also been done, in which the discrimination between these three models with the Λ CDM model may be easily seen. The HDE model shows both quintessence and Chaplygin gas behaviour. The THDE model always lies in the quintessence region while the RHDE model shows the Chaplygin gas behaviour. We hope that in future the model parameters of each DE model can be obtained upon a comparison against several low-redshift observational data such as Pantheon SN Ia data, baryon acoustic oscillations (BAO) and cosmic chronometers (CC) [76–79].

In this work, only statefinder diagnostic tool is used to discriminate the HDE, THDE and RHDE models. Some other diagnostic tools are also available in the literature such as : statefinder hierarchy, growth rate of perturbations, Ω_m diagnostic and $\omega - \omega'$ pair, swampland conjectures [80].

In future work, it is fascinating to make use of these diagnostic tools to differentiate and shed light on the behaviour of various DE models.

Acknowledgements

The authors are highly indebted to the GLA University, India for the support in this academic endeavour.

[1] A. G. Riess *et al.* [Supernova Search Team], “Observational evidence from supernovae for an accelerating uni-

verse and a cosmological constant,” *Astron. J.* **116**, 1009-1038 (1998)

- [2] S. Perlmutter *et al.* [Supernova Cosmology Project Collaboration], “Measurements of Ω and Λ from 42 high redshift supernovae,” *Astrophys. J.* **517** (1999) 565. doi:10.1086/307221 [astro-ph/9812133].
- [3] S. Cole *et al.* [2dFGRS Collaboration], “The 2dF Galaxy Redshift Survey: Power-spectrum analysis of the final dataset and cosmological implications,” *Mon. Not. Roy. Astron. Soc.* **362** (2005) 505. doi:10.1111/j.1365-2966.2005.09318.x
- [4] V. Springel, C. S. Frenk and S. D. M. White, “The large-scale structure of the Universe,” *Nature* **440** (2006) 1137. doi:10.1038/nature04805.
- [5] S. Hanany *et al.*, “MAXIMA-1: A Measurement of the cosmic microwave background anisotropy on angular scales of 10 arcminutes to 5 degrees,” *Astrophys. J.* **545** (2000) L5. doi:10.1086/317322.
- [6] C. B. Netterfield *et al.* [Boomerang Collaboration], “A measurement by Boomerang of multiple peaks in the angular power spectrum of the cosmic microwave background,” *Astrophys. J.* **571** (2002) 604 doi:10.1086/340118.
- [7] L. Amendola, S. Tsujikawa, “Dark energy: theory and observations.” Cambridge University Press (2010).
- [8] L. Amendola, “Dark energy and the Boomerang data.” *Phys. Rev. Lett* **86** 2(2001) 196.
- [9] S. Nojiri and S. D. Odintsov, “The New form of the equation of state for dark energy fluid and accelerating Universe,” *Phys. Lett. B* **639** (2006) 144. doi:10.1016/j.physletb.2006.06.065.
- [10] S. Capozziello, “Dark Energy Models toward observational tests and data”, *Int. J. Geom. Methods Mod. Phys.* **4**(01), (2007) 53-78; K. Bamba, S. Capozziello, S. Nojiri and S. D. Odintsov, “Dark energy cosmology: the equivalent description via different theoretical models and cosmography tests,” *Astrophys. Space Sci.* **342** (2012) 155 doi:10.1007/s10509-012-1181-8.
- [11] S. Vagnozzi, et al. “Do we have any hope of detecting scattering between dark energy and baryons through cosmology?.” *Mon. Not. R. Astron. Soc.* **493** 1(2020): 1139.
- [12] V. Sahni, A. Starobinsky, “The case for a positive cosmological Λ -term,” *Int. J. Mod. Phys. D* **9**(04) (2000) 373-443.
- [13] P. J. E. Peebles and B. Ratra, “The Cosmological constant and dark energy,” *Rev. Mod. Phys.* **75** (2003) 559. doi:10.1103/RevModPhys.75.559
- [14] T. Padmanabhan, “Dark energy and gravity,” *Gen. Rel. Grav.* **40** (2008) 529. doi:10.1007/s10714-007-0555-7; T. Padmanabhan, “Cosmological constant: The Weight of the vacuum,” *Phys. Rept.* **380** (2003) 235. doi:10.1016/S0370-1573(03)00120-0.
- [15] W. Chen and Y. S. Wu, “Implications of a cosmological constant varying as $R^{**(-2)}$,” *Phys. Rev. D* **41** (1990) 695. Erratum: [*Phys. Rev. D* **45**, 4728 doi:10.1103/PhysRevD.41.695].
- [16] S. M. Carroll, “The Cosmological constant,” *Living Rev. Rel.* **4** (2001) 1. doi:10.12942/lrr-2001-1
- [17] E. J. Copeland *et al.*, “Dynamics of dark energy,” *Int. J. Mod. Phys. D* **15** (2006) 1753. doi:10.1142/S021827180600942X
- [18] S. Weinberg, “The Cosmological Constant Problem,” *Rev. Mod. Phys.* **61** (1989) 1. doi:10.1103/RevModPhys.61.1
- [19] A. Sen, “Universality of the tachyon potential,” *J. High Energy Phys.* **1999**(12)(2000) 027.
- [20] P. J. E. Peebles and B. Ratra, “Cosmology with a time-variable cosmological constant,” *Int. J. Mod. Phys. A* **325** (1988) L17-L20.
- [21] M. S. Turner, “Making sense of the new cosmology.” *Int. J. Mod. Phys. A*, **17** (2002) 180.
- [22] T. Chiba, “Tracking K-essence,” *Phys. Rev. D* **66** (2002) 063514. doi:10.1103/PhysRevD.66.063514
- [23] C. Armendariz-Picon, V. Mukhanov, P. J. Steinhardt, “Essentials of k -essence”, *Phys. Rev. D*, **63**(10), (2001) 103510.
- [24] R. R. Caldwell and M. Kamionkowski *et al.*, “Phantom energy and cosmic doomsday,” *Phys. Rev. Lett.* **91** (2003) 071301. doi:10.1103/PhysRevLett.91.071301.
- [25] A. Y. Kamenshchik, U. Moschella *et al.*, “An Alternative to quintessence,” *Phys. Lett. B* **511** (2001) 265. doi:10.1016/S0370-2693(01)00571-8.
- [26] L. Susskind, “The World as a hologram,” *J. Math. Phys.* **36** (1995) 6377 doi:10.1063/1.531249.
- [27] P. Horava and D. Minic, “Probable values of the cosmological constant in a holographic theory,” *Phys. Rev. Lett.* **85** (2000) 1610 doi:10.1103/PhysRevLett.85.1610.
- [28] S. D. Thomas, “Holography stabilizes the vacuum energy,” *Phys. Rev. Lett.* **89** (2002) 081301. doi:10.1103/PhysRevLett.89.081301.
- [29] S. D. H. Hsu, “Entropy bounds and dark energy,” *Phys. Lett. B* **594** (2004) 13 doi:10.1016/j.physletb.2004.05.020.
- [30] M. Li, “A Model of holographic dark energy,” *Phys. Lett. B* **603**, 1 (2004).
- [31] A. G. Cohen, D. B. Kaplan and A. E. Nelson, “Effective field theory, black holes, and the cosmological constant,” *Phys. Rev. Lett.* **82**, 4971 (1999).
- [32] X. Zhang, “Dynamical vacuum energy, holographic quintom, and the reconstruction of scalar-field dark energy,” *Phys. Rev. D* **74**, 103505 (2006).
- [33] C. Tsallis and L. J. L. Cirto, “Black hole thermodynamical entropy,” *Eur. Phys. J. C* **73**, 2487 (2013).
- [34] C. Tsallis, Possible Generalization of Boltzmann-Gibbs Statistics, *J. Stat. Phys.* **52**, 479 (1988).
- [35] C. Tsallis, Black Hole Entropy: A Closer Look. *Entropy*, **22**(1), 17 (2020).
- [36] R. C. Nunes, E. M. Barboza, Jr., E. M. C. Abreu and J. A. Neto, “Probing the cosmological viability of non-gaussian statistics,” *JCAP* **1608**, 051 (2016).
- [37] A. Sayahian Jahromi, S. A. Moosavi, H. Moradpour, J. P. Morais Graa, I. P. Lobo, I. G. Salako and A. Jawad, “Generalized entropy formalism and a new holographic dark energy model,” *Phys. Lett. B* **780**, 21 (2018).
- [38] M. Masi, *Phys. Lett. A* **338**, 217 (2005)
- [39] A. Rnyi, *Probability Theory* (North-Holland, Amsterdam, 1970).
- [40] M. Tavayef, A. Sheykhi, K. Bamba and H. Moradpour, “Tsallis Holographic Dark Energy,” *Phys. Lett. B* **781** (2018) 195 doi:10.1016/j.physletb.2018.04.001.
- [41] H. Moradpour, S. A. Moosavi, I. P. Lobo, J. P. Morais Graa, A. Jawad and I. G. Salako, “Thermodynamic approach to holographic dark energy and the Rényi entropy,” *Eur. Phys. J. C* **78**, 10, 829 (2018).
- [42] E. M. Barboza, Jr., R. d. C. Nunes, E. M. C. Abreu and J. Ananias Neto, “Dark energy models through nonextensive Tsallis statistics,” *Physica A* **436** (2015) 301.
- [43] C. Tsallis, “The nonadditive entropy S_q and its applications in physics and elsewhere: Some remarks,” *Entropy* **13** (2011) 1765.

- [44] M. A. Zadeh, A. Sheykhi and H. Moradpour and K. Bamba, "Note on Tsallis holographic dark energy," *Eur. Phys. J. C* **78**, (2018) 940.
- [45] S. Ghaffari et al., "Tsallis holographic dark energy in the brane cosmology," *Phys Dark Univ* **23**, (2019) 100246.
- [46] U. K. Sharma and V. C. Dubey, "Interacting Rényi holographic dark energy with parametrization on the interaction term," arXiv:2001.02368 [gr-qc].
- [47] S. Ghaffari et al., "Inflation in the Rényi cosmology." *Mod. Phys. Lett. A* **35**, (2020) 1950341
- [48] S. Nojiri, S. D. Odintsov and E. N. Saridakis, "Modified cosmology from extended entropy with varying exponent," *Eur. Phys. J. C* **79** (2019) 242.
- [49] A. Sheykhi, "Modified Friedmann equations from Tsallis entropy," *Phys. Lett. B* **785** (2018) 118.
- [50] Q. Huang, H. Huang, J. Chen, L. Zhang and F. Tu, "Stability analysis of a Tsallis holographic dark energy model," *Class. Quant. Grav.* **36**, no. 17, (2019) 175001.
- [51] E. Sadri, "Observational constraints on interacting Tsallis holographic dark energy model," *Eur. Phys. J. C* **79** 9 (2019) 762.
- [52] R. D'Agostino, "Holographic dark energy from nonadditive entropy: cosmological perturbations and observational constraints," *Phys. Rev. D* **99** 10(2019) 103524.
- [53] V. C. Dubey, S. Srivastava, U. K. Sharma and A. Pradhan, "Tsallis holographic dark energy in Bianchi-I Universe using hybrid expansion law with k -essence," *Pramana* **93** 5, 78 (2019).
- [54] M. Abdollahi Zadeh, A. Sheykhi, H. Moradpour and K. Bamba, "Effects of Anisotropy on the Sign-Changeable Interacting Tsallis Holographic Dark Energy," *Mod. Phys. Lett. A* **33** (2020) 2050053.
- [55] E. N. Saridakis, K. Bamba, R. Myrzakulov and F. K. Anagnostopoulos, "Holographic dark energy through Tsallis entropy," *JCAP* **1812** (2018) 012.
- [56] A. Dixit, U. K. Sharma and A. Pradhan, "Tsallis holographic dark energy in FRW Universe with time varying deceleration parameter," *New Astron.* ,**73**101281 (2019).
- [57] M. Abdollahi Zadeh, A. Sheykhi and H. Moradpour, "Thermal stability of Tsallis holographic dark energy in nonflat Universe," *Gen. Rel. Grav.* **51** 1, (2019) 12 .
- [58] S. Ghaffari, E. Sadri and A. H. Ziaie, "Tsallis holographic dark energy in Fractal Universe," arXiv:1908.10602 [gr-qc].
- [59] A. Jawad, S. Rani and N. Azhar, "Non-flat FRW universe version of Tsallis holographic dark energy in specific modified gravity," *Mod. Phys. Lett. A* **34** (2019) 1950055.
- [60] V. C. Dubey, et al. "Tsallis holographic dark energy Models in axially symmetric space time." *Int. J. Geom. Methods Mod. Phys.* **17** 1 (2020) 2050011.
- [61] Y. Aditya, S. Mandal, P. K. Sahoo and D. R. K. Reddy, "Observational constraint on interacting Tsallis holographic dark energy in logarithmic BransDicke theory," *Eur. Phys. J. C* **79**12, 1020 (2019).
- [62] V. Sahni et al., "Statefinders a new geometrical diagnostic of dark energy" *JETP Lett.* **77**(5), (2003) 201.
- [63] U. Alam et al., "Exploring the expanding universe and dark energy using the Statefinder diagnostic," *Mon. Not. R. Astron. Soc.* **344**(4), (2003) 1057.
- [64] C. J. Feng, "Statefinder diagnosis for Ricci dark energy" *Phys. Lett. B* **670**(3), (2008).
- [65] Z. L. Yi et al., "Statefinder diagnostic for the modified polytropic Cardassian universe" *Phys. Rev. D* **75**(8) (2007) 083515.
- [66] X. Zhang, "Statefinder diagnostic for holographic dark energy model" *Int. J. Mod. Phys. D* **14**(09), (2005) 1597.
- [67] U. K. Sharma and A. Pradhan, "Diagnosing Tsallis holographic dark energy models with statefinder and $\omega - \omega'$ pair" *Mod. Phys. Lett. A* **34**(13) (2019) 1950101.
- [68] G. Varshney et al., "Statefinder diagnosis for interacting Tsallis holographic dark energy models with $\omega - \omega'$ pair" *New Astron.* **70**, (2019) 36.
- [69] V. C. Dubey, U. K. Sharma, A. Beesham, "Tsallis holographic model of dark energy: Cosmic behavior, statefinder analysis and $\omega_D - \omega'_D$ pair in the non-flat universe", *Int. J. Mod. Phys. D* **1528** (2019) 1950164. arXiv preprint arXiv:1905.02449
- [70] U. K. Sharma, V. C. Dubey, A. Pradhan, "Diagnosing interacting Tsallis holographic dark energy in the non-flat universe", *Int. J. Geom. Meth. Mod. Phys.*, **17**(2), 2050032 (2020). <https://doi.org/10.1142/S0219887820500322>
- [71] S. Srivastava, V. C. Dubey, U. K. sharma, "Statefinder diagnosis for Tsallis ageographic dark energy model with $\omega_D - \omega'_D$ pair," *Int. J. Mod. Phys. A* **35**, 2050027 (2020).
- [72] J. L. Cui, J. F. Zhang, "Comparing holographic dark energy models with statefinder," *Eur. Phys. J. C* **74**(4), 2849 (2014).
- [73] S. Wang, Y. Wang and M. Li, "Holographic dark energy," *Phys. Rept.* 696, 1 (2017).
- [74] Y. H. Li, S. Wang, X. D. Li and X. Zhang, "Holographic dark energy in a Universe with spatial curvature and massive neutrinos: a full Markov Chain Monte Carlo exploration," *JCAP* **02** (2013), 033
- [75] U. K. Sharma and V. C. Dubey, "Statefinder diagnostic for the Rényi holographic dark energy," *New Astron.* **80** (2020), 101419
- [76] V. V. Lukovi, B. S. Haridasu and N. Vittorio, "Cosmological constraints from low-redshift data," *Found. Phys.* **48**, no.10, 1446-1485 (2018)
- [77] V. V. Lukovi, B. S. Haridasu and N. Vittorio, "Exploring the evidence for a large local void with supernovae Ia data," *Mon. Not. Roy. Astron. Soc.* **491**, no.2, 2075-2087 (2020)
- [78] B. S. Haridasu, V. V. Lukovi, M. Moresco and N. Vittorio, "An improved model-independent assessment of the late-time cosmic expansion," *JCAP* **10**, 015 (2018)
- [79] R. D'Agostino, "Holographic dark energy from nonadditive entropy: cosmological perturbations and observational constraints," *Phys. Rev. D* **99**, no.10, 103524 (2019)
- [80] S. Brahma and M. W. Hossain, "Dark energy beyond quintessence: Constraints from the swampland," *JHEP* **06**, 070 (2019)